2024 European Control Conference (ECC)
June 25-28, 2024. Stockholm, Sweden

Energy-optimal trajectory planning for electric vehicles using Model Predictive Control

Alexandre Rocha*[1], Anand Ganesan[1,2], Derong Yang[2], and Nikolce Murgovski[1]

Abstract— **This paper proposes a space-sampled Economic Model Predictive Control (EMPC) approach to jointly minimize total energy consumption of an electric vehicle (EV) and track both longitudinal velocity and path curvature reference trajectories. We consider a single-track vehicle model constrained to the range of accelerations ± 3 m/s^2, and energy consumption is modelled explicitly including power losses of electric machines. Simulations with the high-fidelity simulator IPG CarMaker show the trade-off between energy consumption and reference tracking. Namely, results show how longitudinal velocity and acceleration control significantly impact energy consumption, whereas deviating from the path centerline mainly allows better velocity tracking.**

I. Introduction

The automotive industry is undergoing a disruptive transformation in the last two decades, empowered by economic, regulatory, and sustainability drivers. From policy makers to consumers, society in general has created incentives to develop less polluting and more efficient means of transportation, and manufacturers are rapidly adapting [1]. Electric vehicles (EVs) appear as one such solution that reduces air pollution throughout the energy production and consumption cycle [2]. Although electric motors used in EVs are incomparably more efficient than internal combustion engines, current state-of-the-art batteries have a significantly lower energy density than fossil fuels, leading to reduced driving range. As a solution, alongside development of battery technology, energy management can be embedded in vehicle motion control algorithms [3], resulting in energy-optimal driving of EVs.

According to the vehicle's level of control autonomy, energy consumption optimization occurs at different levels of the control architecture and is embedded in different types of algorithms. Cruise control (CC) emerges as one of the most widely implemented of such algorithms. It consists of autonomously tracking a reference longitudinal velocity, while the driver remains responsible for the vehicle's steering. CC can be energy-optimal when taking into account an energy consumption model and information about the surrounding environment, such as traffic ahead and road slope [4], [5]. If a vehicle autonomously controls its motion, then the problem is converted to trajectory tracking or planning. Trajectory tracking consists of jointly tracking given path and velocity references [6], [7]. Commonly, these algorithms focus on accurately tracking the references, which can be energy-optimal based on route prior knowledge - a problem known as route planning. Instead, trajectory planning deals with computing the vehicle's position and velocity trajectories online, given local and real-time information, possibly optimizing certain performance objectives. The well-known work of [8] is an illustrative example of when multiple traffic scenarios demand iterative replanning of trajectories. Other traffic scenarios in which trajectory planning is applied include obstacle avoidance [9], [10], as well as overtaking and road merging maneuvers [11], [12]. Moreover, analogous to CC, trajectory planning is energy-optimal when energy consumption is modelled and optimized in the planning problem [13], [14].

Optimizing the trajectory in real-time requires one to solve numerically and iteratively an optimal control problem (OCP) as the vehicle moves and acquires new information. In contrast to low-speed autonomous vehicles, such as in certain industrial applications, road EVs require high-frequency control updates to meet safety, comfort, and drivability standards, which has been limiting the research focus of this topic. Until today, most energy management strategies did not include the joint problem of trajectory planning and energy consumption minimization, where instead a subproblem is considered, for example, energy-optimal cruise control. Moreover, from the reduced set of works that do include such joint problem, energy consumption is not always modelled explicitly, where commonly an approximation of it is considered, thus being suboptimal. Nevertheless, as the computational power of vehicle embedded systems increases, energy optimization problems become feasible to compute in real time [3], with higher modelling accuracy, and integrated into more complex vehicle motion control algorithms [15].

In this paper, we address the problem of energy-optimal trajectory planning of an electric vehicle by explicitly modelling the vehicle powertrain energy consumption. This consumption model includes the power losses of electric motors and their inverters, which are fitted to measured efficiency points. The trajectory is then optimized to minimize total energy consumption while tracking longitudinal velocity and road curvature references. Furthermore, we study the relative impact of these tracking objectives on energy consumption by allowing the vehicle to deviate from the references. From the control perspective, the MPC framework is chosen due to its ability to encompass a dynamic model of the vehicle to predict its future motion, handle constraints, and optimize specific performance criteria in an integrated feedback loop. To limit computational complexity, the focus is placed on constrained-acceleration scenarios, avoiding cumbersome nonlinearities within the vehicle model that might lead to MPC feasibility problems and high computational times.

[1]Dept. of Electrical Engg., Chalmers University of Technology, Göteborg, Sweden. {rochaa,anandg,nikolce.murgovski}@chalmers.se
[2]Dept. of Software Engg., R&D, Volvo Cars, Göteborg, Sweden {anand.ganesan,derong.yang}@volvocars.com

Furthermore, inspired by [9], [10], vehicle kinematics is modelled relative to the path and the MPC problem is reformulated into the spatial domain, both of which largely simplify problem formulation. Path curvature depends implicitly on velocity in the temporal domain, and thus on the actuators. As a consequence, not only the integration of the dynamics increase in complexity but also the constraints on path boundaries become time-dependent. By changing the sampling domain from time to space, path boundaries and curvature are defined as functions of the independent variable, avoiding the intricate dependence on vehicle velocity. Finally, the proposed algorithm is tested in a test track on the high-fidelity vehicle simulator IPG CarMaker, where simulations are conducted for different controller tuning to illustrate the trade-off between energy consumption and reference tracking.

II. System modelling

The vehicle chassis is a rigid body with mass m and rotational inertia I_z and its position is described in the curvilinear coordinate system, which relates the chassis center of mass to a reference path. The degree of model accuracy must be weighted with the complexity arising from nonlinearities and increase in state-space dimension, in order to achieve a reasonable trade-off with computational burden. In this paper, a compromise is found by limiting the vehicle operating range, constraining vehicle accelerations, which allows for model simplification. To start with, the chassis model includes only one wheel per axle. Consequently, roll dynamics are ignored, whereas pitch, and thus longitudinal load transfer, are assumed static. Furthermore, the tire traction forces are modelled as linear, and the wheel dynamics is neglected. The control inputs are the steering rate $\dot{\delta}$ of the front axle and the total propulsion torque rate $\dot{T}$, whereas friction brakes are not considered.

Regarding the power consumption model, we consider the total mechanical output power from the electric motors together with the power losses of the electric machines, i.e. motors and inverters, which vary depending on motor speed and torque. Furthermore, in this paper, the subscript $i = \{f, r\}$ indicates the front (f) and rear (r) wheel, and the constant positive parameters of the vehicle model are denoted using the symbol C with a suitable subscript.

A. Curvilinear bicycle model

The curvilinear bicycle model (or single-track model) is illustrated in Fig. 1. Vehicle kinematics is defined relative to the path centerline, whereas its dynamics follows the single-track model [16]. Let the kinematic states s, d, and $\Delta\psi = \psi - \psi_s(s)$ denote the distance travelled along the path, the lateral displacement from the given path centerline, and the local heading angle, respectively, where $\psi_s(s)$ denotes the heading of the path at s. Moreover, let $\kappa(s)$ be the curvature of the path centerline at s. Using this coordinate system, there is no need for the absolute $x - y$ position. Instead, we consider longitudinal and lateral velocities, v_x and v_y, and the yaw rate r. Given a planar road with zero slope and bank

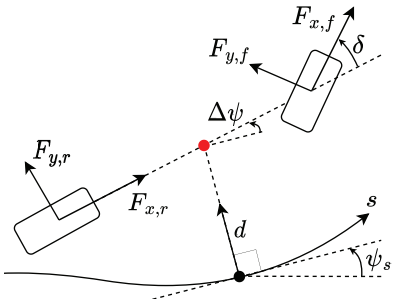

Fig. 1. Vehicle representation in the curvilinear coordinate system.

angles, the resulting vehicle kinematics and dynamics are as in [17] and [16], respectively:

$$\begin{aligned}
\dot{s} &= \frac{v_x \cos(\Delta\psi) - v_y \sin(\Delta\psi)}{1 - \kappa(s)d} \ , \\
\dot{d} &= v_x \sin(\Delta\psi) + v_y \cos(\Delta\psi) \ , \\
\Delta\dot{\psi} &= r - \kappa(s)\dot{s} \ , \\
m\dot{v}_x &= \cos(\delta)F_{x,f} - \sin(\delta)F_{y,f} + F_{x,r} + mv_y r - F_{\mathrm{d}} \ , \\
m\dot{v}_y &= \cos(\delta)F_{y,f} + \sin(\delta)F_{x,f} + F_{y,r} - mv_x r \ , \\
I_z\dot{r} &= l_f \cos(\delta)F_{y,f} + l_f \sin(\delta)F_{x,f} - l_r F_{y,r} \ ,
\end{aligned} \tag{1}$$

where $F_{x,i}$ and $F_{y,i}$ are the longitudinal and lateral tire forces, δ is the steering angle, l_i is the distance from the center of mass to the wheel i, and F_d are the dissipative forces.

Given the absence of wheel dynamics, the longitudinal tire forces are linear on motor torque, T: $F_{x,i} = TC_{T,i}$, where $C_{T,i}$ considers the gear ratio, the wheel radius, and the torque distribution among axles. Whereas, the lateral tire forces result from a linearization of Pacejka's tire model [18], $F_{y,i} = C_y\sigma_{y,i}$, where $\sigma_{y,i} = -\arctan(\frac{v_{y,i}}{v_{x,i}})$ is the lateral slip angle of the tires that depends on the longitudinal and lateral velocities, $v_{x,i}$ and $v_{y,i}$, in the wheel coordinate frame. The parameter C_y is the slope of Pacejka's tire model at zero tire slip and is scaled according to the normal load on each wheel: $F_{z,f} = \frac{mgl_r}{l_f+l_r}$ and $F_{z,r} = \frac{mgl_f}{l_f+l_r}$, where g stands for gravity.

The dissipative forces are the aerodynamic drag force $F_{\text{aero}} = C_{\text{aero}}v_x^2$ (wind speed and direction are neglected) and the tire rolling resistance force $F_{rr_i} = C_{\text{rr}}F_{z,i}$.

B. Power consumption

Let ω and T stand for motor rotational speed and torque. The total power consumption at a given time instant is

$$P = P_{\text{mech}} + P_{\text{el.loss}} = wT + P_{\text{el.loss}} \ , \tag{2}$$

where P_{mech} is the mechanical power output of the motor and $P_{\text{el.loss}}$ stands for the power losses of the electric machines.

According to the modelled dynamics, the power produced by the motor to overcome all resistive forces, P_{mech}, is decomposed into inertial power (wheel rotational inertia neglected) and power losses due to tire resistive forces related to rolling resistance and lateral slip, and aerodynamic drag. Power losses in electric motors and their inverters,

$P_{\text{el.loss}}$, are modelled as a polynomial fit of the efficiency operating points, measured experimentally. In this work, the polynomial is of 5th and 2nd order in motor rotational speed, ω, and in its torque, T, respectively,

$$P_{\text{el.loss}}(\omega, T) = \sum_{n=0}^{5} \sum_{m=0}^{2} p_{n,m} w^n T^m \ , \tag{3}$$

$p_{(\cdot,\cdot)}$ being fitting parameters and $p_{4,2} = p_{5,1} = p_{5,2} = 0$

C. Optimal Control Problem (OCP)

The problem is formulated as an economic optimal control problem (OCP), where the main objective is to track a reference longitudinal velocity trajectory and the path centerline while minimizing energy consumption.

Let the system state $\mathbf{x}$ and input $\mathbf{u}$ vectors be:

$$\mathbf{x} = \begin{bmatrix} s & d & \Delta\psi & v_x & v_y & r & \delta & T \end{bmatrix}^T \ , \tag{4}$$

$$\mathbf{u} = \begin{bmatrix} \dot{\delta} & \dot{T} \end{bmatrix}^T \ . \tag{5}$$

The respective dynamics $f(\mathbf{x}(t), \mathbf{u}(t), \kappa(s(t)))$ are then as in Eq. (1), with the addition that the steering angle and motor torque are lifted to match the system input with the controlled variable of the actuators.

Recall that the validity region of this vehicle model is limited when compared to a high-fidelity counterpart. For that reason, a_x and a_y are constrained to a reduced operating range. In addition, $[\delta, \dot{\delta}, T, \dot{T}, d]$ are also constrained according to the physical limitations of both the actuators and the track. These are modelled as constant-value box constraints except for d, which is constrained according to the time-dependent bounds.

Given an obstacle-free feasible path, whose curvature and bounds are known a priori, the problem is formulated as:

$$\begin{aligned}
\min_{\mathbf{x}(t),\mathbf{u}(t)} \ & \int_0^{t_f} l(\mathbf{x}(\tau), \mathbf{u}(\tau)) \, \mathrm{d}\tau + m(\mathbf{x}(t_f)) \\
\text{s.t.} \quad & \dot{\mathbf{x}}(t) = f(\mathbf{x}(t), \mathbf{u}(t), \kappa(s(t))), \ \forall t \in [0, t_f[, \\
& \mathbf{x}(t) \in [\underline{\mathbf{x}}, \bar{\mathbf{x}}], \quad \forall t \in [0, t_f], \\
& \mathbf{u}(t) \in [\underline{\mathbf{u}}, \bar{\mathbf{u}}], \quad \forall t \in [0, t_f[, \\
& g(\mathbf{x}(t), \mathbf{u}(t), \kappa(s(t))) \leq 0, \quad \forall t \in [0, t_f[, \\
& \mathbf{x}(0) = \hat{\mathbf{x}}_0, \ \mathbf{x}(t_f) \in \mathcal{X},
\end{aligned} \tag{6}$$

where $l(\cdot)$ and $m(\cdot)$ are generalized running and target cost functions, the notation $\{\underline{\alpha}, \bar{\alpha}\}$ refer to the lower and upper bound of α, and $g(\cdot)$ denotes additional algebraic constraints on acceleration. The initial state is set as the path initial state $\hat{\mathbf{x}}_0$ and the final state is constrained to the target set $\mathcal{X}$.

III. Numerical Solution of OCP

The optimal control problem (6) is solved numerically, in a receding horizon fashion. The problem is first reformulated in the spatial domain and then transcribed into a nonlinear finite-dimension optimization problem, which is then solved by a state-of-the-art numerical solver at every control iteration. We use the software acados [19] for problem formulation, and the solver numerical method is the Sequential Quadratic Programming, which uses an interior-point method solver, HPIPM [20], to solve each sub-quadratic program.

A. Spatial reformulation of system dynamics

By changing the sampling domain, the system dynamics becomes a function of track progress s instead of time t. Subsequently, s becomes both the independent variable and a state, being thus possible to reduce the state vector to

$$\xi = \begin{bmatrix} d & \Delta\psi & v_x & v_y & r & \delta & T \end{bmatrix}^T \ , \tag{7}$$

whose dynamics $f_s(\xi(s), \mathbf{u}(s), \kappa(s))$ in the spatial domain are defined $\forall \dot{s} \neq 0$ as follows:

$$\begin{aligned}
\frac{\partial \xi(t)}{\partial s} &= \frac{\partial \xi(t)}{\partial t} \frac{\partial t}{\partial s(t)} = f(\xi(t), \mathbf{u}(t), \kappa(s(t))) \frac{1}{\dot{s}(t)} \\
&= f_s(\xi(s), \mathbf{u}(s), \kappa(s)).
\end{aligned} \tag{8}$$

There are a set of advantages inherent to this sampling domain. Firstly, reducing the dimension of the state-space formulation reduces problem dimensionality and, consequently, its computational expenditure. Secondly, path curvature becomes a function of the independent variable, avoiding an intricate dependency on time and, in turn, numerical instability when integrating dynamics. Lastly, formulation of constraints on d is simplified. Whereas in the temporal domain, the nearest boundary depends on velocity, in the spatial domain it is constant at every sampling instant. As disadvantages, the spatial domain introduces a singularity at $\dot{s} = 0$ and increases the nonlinearity of f_s due to multiplication with $\frac{1}{\dot{s}(t)}$.

B. MPC Problem Formulation

A direct multiple shooting is used as a transcription method, discretizing the state and the input space into a regular finite-sized grid. The implicit 4th-order Runge-Kutta method is used to discretize system dynamics, and hereon we denote their discrete counterpart as $f_s^d(\xi(s), \mathbf{u}(s), \kappa(s))$.

The receding horizon optimization problem is an economic MPC (EMPC) problem, and it is solved for a finite-horizon of S_f and a horizon length N, with sampling interval $\Delta s = S_f/N$. In EMPC, persistent feasibility is cumbersome to guarantee, and operating near feasibility limits may increase computational complexity. To avoid such difficulties, the constraints the vehicle most often tends to violate, i.e. those of acceleration and path limits, are softened by adding slack variables, represented by the vector ζ, and penalizing them. Let the subscript i denote the node i of the horizon starting at s_0, thus abbreviating $\alpha(i|s_0)$ to α_i. The EMPC problem formulation then follows:

$$\begin{aligned}
\min_{\substack{\xi_0,\dots,\xi_N,\mathbf{u}_1,\dots,\\ \mathbf{u}_{N-1},\zeta_1,\dots,\zeta_N}} \ & \sum_{i=0}^{N-1} \Big(\|\xi_i - \xi_{i,\text{ref}}\|^2_{Q_\xi} + \|\mathbf{u}_i\|^2_{Q_u} \\
& \quad + \|a_{x,i}\|^2_{q_{a_x}} + \|\zeta_i\|^2_{Q_\zeta} + q_{e,i} E_i \Big) \\
& \quad + \|\xi_N - \xi_{N,\text{ref}}\|^2_{Q_x} + \|\zeta_N\|^2_{Q_\zeta} \\
\text{s.t.} \quad & \xi_{i+1} = f_s^d(\xi_i, \mathbf{u}_i, \kappa_i(s_i)), \ \forall i \in [0, N-1] \\
& \xi_i \in [\underline{\xi}, \bar{\xi}], \quad \forall i \in [0, N] \\
& \mathbf{u}_i \in [\underline{\mathbf{u}}, \bar{\mathbf{u}}], \quad \forall i \in [0, N-1] \\
& g_s(\xi_i, \mathbf{u}_i, \kappa(s_i)) \leq 0, \quad \forall i \in [0, N-1] \\
& \xi_0 = \hat{\xi}(s_0) \ ,
\end{aligned} \tag{9}$$

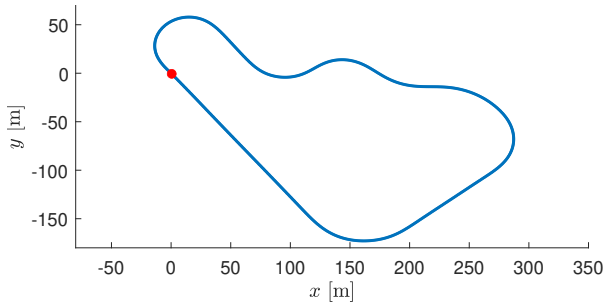

Fig. 2. Test path with initial point highlighted in red.

where $E = P\Delta s/\dot{s}$ is the energy consumed per sampling interval and $\hat{\xi}(s_0)$ is the measured current state. Constrained variables are those referred to in Section II-C, where the algebraic constraints are redefined in the spatial domain as $g_s(\cdot)$. Specifically, algebraic constraints limit the longitudinal and lateral accelerations as $a^2_{(\cdot)} \leq 3^2\text{m/s}^2$. To mitigate tuning unbalance between terms of different units and magnitude in the cost functions, the weights $q_\cdot$ and $Q_\cdot$ are scaled as follows:

$$Q_{\xi,1,1} = \frac{\tilde{q}_d}{d^2_{\max}},\ Q_{\xi,3,3} = \frac{\tilde{q}_v}{(v_x - v_{x,\text{ref}})^2_{\max}},\ Q_{\mathbf{u},1,1} = \frac{\tilde{q}_{\dot{\delta}}}{\dot{\delta}^2_{\max}}$$
$$Q_{\mathbf{u},2,2} = \frac{\tilde{q}_{\dot{T}}}{\dot{T}^2_{\max}},\ q_{a_x} = \frac{\tilde{q}_{a_x}}{a^2_{x,max}},\ q_{e,i} = \frac{\tilde{q}_e}{v_{x,\text{ref},i} C_E T_{\max}}\ ,$$

where $Q_{(\cdot)}$ are diagonal matrices with $Q_{\xi,n,n} = 0\,\forall n \in \{2,4,5,6,7\}$, $(v_x - v_{x,\text{ref}})_{\max}$ is user-defined, and the constant C_E translates linear wheel velocity to motor rotation velocity.

IV. Simulation Results

The proposed controller was tested with a high-fidelity model of a sports passenger car in the IPG CarMaker software. The main parameters of the vehicle are: $m = 2100$ kg, $I_z = 4900$ kg/m^2, and $l_f + l_r = 2.80$ m. Moreover, it has one electric motor per each wheel, among which the optimized torque is equally distributed. The test track is presented in Fig. 2. It is a planar path with constant width and multiple corners of increasing curvature. The vehicle starts at the red dot in Fig. 2 and drives towards the first corner to the left. At the start of every simulation, the vehicle is driven from $v_x = 0$ km/h towards the reference velocity by the controller embedded in the simulator. MPC takes control only after the vehicle velocity is close enough to the reference velocity. All plots below contain a vertical line that indicates the MPC trigger instant. Furthermore, we assume full-state observation and the controller runs at 20 Hz. All computations were performed on a standard laptop computer with Intel i9 2.30 GHz processor.

The reference $\xi_{\text{ref}}(s)$ is composed by zero-elements except for the reference longitudinal velocity, which is defined as:

$$v_{x,\text{ref}}(s) = \min\left\{V_{x,\text{ref}}, \sqrt{\frac{a_{y,\max}}{\|\kappa(s)\|}}\right\}\ , \qquad (10)$$

where $V_{x,\text{ref}}$ is a constant velocity reference value. By saturating $V_{x,\text{ref}}$ according to $\kappa(s)$ and $a_{y,\max}$, we ensure the optimal velocity trajectory remains in the vicinity of the reference. Although this saturation can be less accurate for $d \neq 0$, it is assumed to have little effect on the optimal trajectory and to be surmountable with proper controller tuning.

TABLE I
Energy-optimal path tracking: Performance indicators

$\{\tilde{q}_{a_x}, \tilde{q}_e\}$	$\{0,0\}$	$\{0,10\}$	$\{1,0\}$	$\{1,10\}$
Relative energy saving [%]	-	0.0	12.1	14.2
$\bar{v}_x$ [km/h]	44.9	44.9	44.1	43.9
MAD (d) [m]	0.06	0.05	0.06	0.06
Mean computation time [ms]	7.7	15.2	7.4	14.6
Max computational time [ms]	15.0	21.4	13.8	24.0

Two scenarios are studied. Firstly, MPC is tuned to accurately track the path centerline, where different values of $\tilde{q}_e$ and $\tilde{q}_{a_x}$ are chosen to analyze the impact of longitudinal control on energy savings. Secondly, a range of $\tilde{q}_d$ is chosen to study the effect of deviating from the path centerline on energy consumption. We refer to these scenarios as energy-optimal path tracking and trajectory planning, respectively. In both, the reference velocity is $V_{x,\text{ref}} = 70$ km/h, and the look-ahead distance is $S_f = 50$ m with $N = 50$.

In the results, the energy consumed along the path is decomposed into different sources of consumption, computed for the high-fidelity vehicle model. These are inertial forces (linear and rotational), tire resistive forces (longitudinal and lateral slips and rolling resistance), and aerodynamic drag. Other types of non-modelled power dissipation sources, e.g. gears, are assumed negligible due to their magnitude.

A. Energy-optimal path tracking

The controller is tuned with the following parameters:

$$\tilde{q}_d = 10,\ \tilde{q}_v = 1,\ \tilde{q}_{\dot{\delta}} = 0.1,\ \tilde{q}_{\dot{T}} = 0.05,$$
$$\tilde{q}_{a_x} \in \{0,1\},\ \tilde{q}_e \in \{0,10\}\ .$$

The tracking results are shown in Fig. 3 and the performance indicators for this scenario are summarized in Table I. Looking at the latter, one can note that the mean absolute deviation of d from $d = 0$, MAD(d), is similarly low for all $\{\tilde{q}_e, \tilde{q}_{a_x}\}$, which indicates the vehicle accurately tracks the path centerline. Given the high $\tilde{q}_d$, the controller is expected to exploit v_x instead in order to save energy. Nevertheless, in Fig. 3, comparing the two trajectories with $\tilde{q}_{a_x} = 0$, higher $\tilde{q}_e$ did not lead to a significant reduction in velocity - the trajectories practically overlap. In fact, for that $\tilde{q}_{a_x}$, trajectories show aggressive manoeuvring to track the reference, which in turn is infeasible given the constraints on acceleration. Conversely, when $\tilde{q}_{a_x} = 1$, the overall penalty on deviating from $v_{x,\text{ref}}$ is reduced and one observes a slight, but visible difference between trajectories for different $\tilde{q}_e$.

Comparing results with different $\tilde{q}_{a_x}$, one concludes that smoother longitudinal control yielded a lower overall energy consumption. Penalizing $\tilde{q}_{a_x}$ resulted in fewer electrical and longitudinal tire slip power losses, where a reduction of $\bar{v}_x \approx 1$ km/h also led to a decrease in drag power losses and inertial power. The energy dissipated due to rolling resistance remained constant, since load transfer is assumed

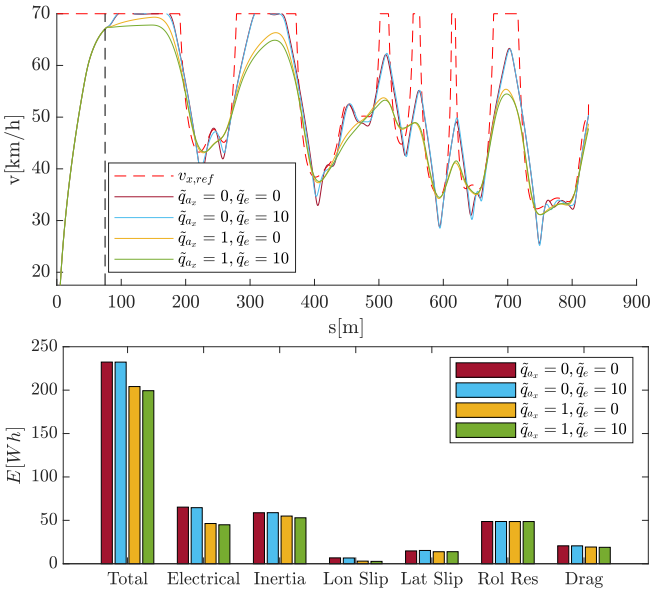

Fig. 3. Energy-optimal path tracking: Longitudinal velocity and energy consumption (per dissipation source). "Lon Slip" and "Lat Slip" refer to longitudinal and lateral tire slips, and "Rol Res" refers to tire rolling resistance.

static, while dissipation due to tire lateral slip did not vary significantly and was of low magnitude due to the limited range of lateral accelerations.

Having as a baseline the case with $\{\tilde{q}_{a_x}, \tilde{q}_e\} = \{0, 0\}$, smoothing vehicle accelerations and reducing $\bar{v}_x \approx 1$ km/h led to energy savings of more than 12%. More interestingly, comparing the trajectories with $\tilde{q}_{a_x} = 1$ but different $\tilde{q}_e$, it was found that reducing acceleration when entering and exiting corners while reducing speed on average solely 0.2 km/h, resulted in consuming 2.1% less energy.

Furthermore, maximum computation did not exceed two times the average, which suggests solver numerical stability. It is also interesting to note that including the economic term in MPC led to higher computation times, illustrating its impact on computational complexity.

B. Energy-optimal trajectory planning

For this study, multiple simulations were conducted for different $\tilde{q}_e$ and $\tilde{q}_d$, with the following MPC tuning:

$$\tilde{q}_v = 1, \tilde{q}_{a_x} = 1, \tilde{q}_{\dot{\delta}} = 0.1, \tilde{q}_{\dot{T}} = 0.05$$
$$\tilde{q}_d = 10^n,\ n \in \{-4, -3, ..., 2\},\ \tilde{q}_e \in \{2, 5, 10\}.$$

Fig. 4 illustrates a set of performance indicators of all simulated trajectories: energy consumption E, MAD(d), $\bar{v}_x$, MAD of v_x from $v_{x,\text{ref}}$, a_x standard deviation, $\sigma(a_x)$, and the closed-loop trajectories cost, J.

Looking at the evolution of the different parameters as a function of $\tilde{q}_d$, one concludes that the energy consumed over one lap increased as $\tilde{q}_d$ decreased. Fig. 5 presents an analysis of two trajectories corresponding to $\tilde{q}_d \in \{10^{-4}, 10\}$, with constant $\tilde{q}_e = 10$, which illustrate the following conclusions. For high $\tilde{q}_d$, the main objective of the vehicle is to follow the centerline of the path. To do so, it compromises velocity to guarantee feasible accelerations, which leads to a decrease

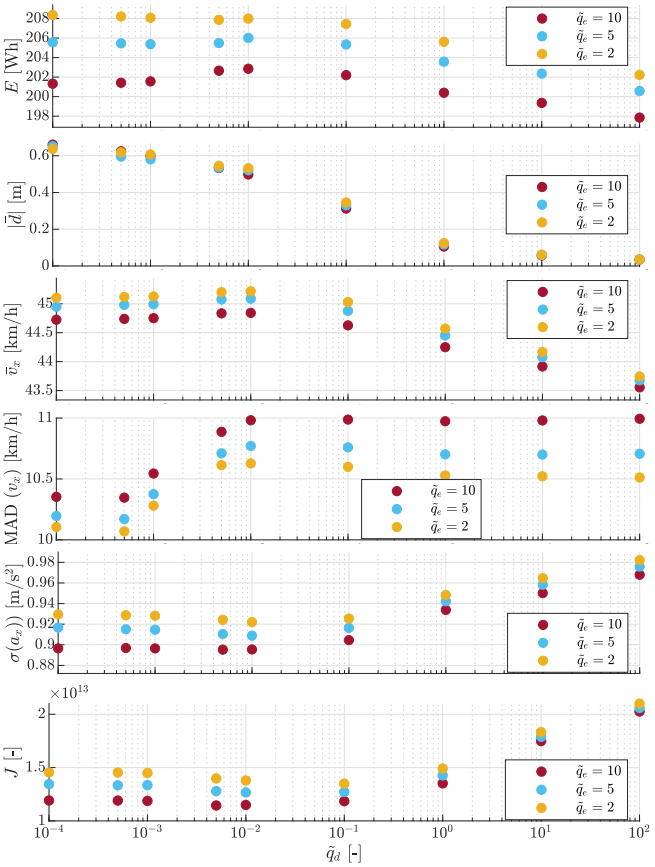

Fig. 4. Energy-optimal trajectory planning: Trade-off between reference tracking and energy consumption.

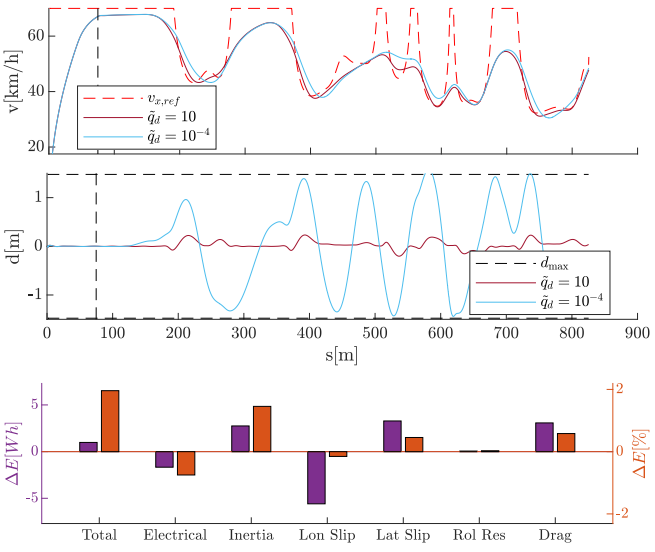

Fig. 5. Energy-optimal trajectory planning: Longitudinal velocity, lateral displacement, and energy consumption per dissipation source with $\tilde{q}_d = 10^{-4}$ relative to the baseline $\tilde{q}_d = 10$.

in $\bar{v}_x$. Coherently with the findings above, such reduction in average velocity led to energy savings, mainly due to lower inertial power and drag power losses. Conversely, for small $\tilde{q}_d$, when approaching a corner, the vehicle both reduces its velocity and deviates from the path centerline. That results in lower longitudinal acceleration and reduced MAD(v_x), since lateral acceleration limits can be respected

by controlling both trajectory curvature and velocity - see Eq. (10). However, even though the electric power losses were of lower magnitude, the higher $\bar{v}_x$ increased the inertial power and drag power losses and consequently the total energy consumption.

The results show a trade-off between energy consumption and reference tracking. The main optimization objective is to track the reference longitudinal velocity, since otherwise the vehicle would have no incentive to move forward. Therefore, energy minimization and tracking of the path centerline become secondary. When reducing the penalty on d, the controller was able to more accurately track $v_{x,\text{ref}}$, increasing $\bar{v}_x$. Moreover, the standard deviation of longitudinal acceleration decreased with $\tilde{q}_d$ due to less variation in the velocity along the track. Consequently, better tracking of $v_{x,\text{ref}}$, smoother longitudinal control, and reduced penalty on d led to an overall decrease in the cost of closed-loop trajectories, at the cost of higher energy consumption. Inversely, the accurate tracking of path centerline increased the cost J due to a higher deviation from $v_{x,\text{ref}}$ and more aggressive longitudinal control, regardless of the decrease in energy consumption. In sum, note that energy consumption depended mainly on $\bar{v}_x$, following a proportional relation to it.

When comparing among $\tilde{q}_e$, instead, the main observation is that the average longitudinal velocity and standard deviation of the longitudinal acceleration decrease as the energy becomes more expensive for higher $\tilde{q}_e$, resulting in lower J. However, attention must be paid when increasing $\tilde{q}_e$, since too high values can lead to deviation from $v_{x,\text{ref}}$ in straight parts of the track, which is obviously undesirable.

V. Conclusions

In this paper, we proposed an Economic Model Predictive Control (EMPC) approach to the problem of energy-optimal trajectory planning of an electric vehicle. A simplified vehicle dynamics model was presented, and the problem was formulated in the spatial domain, which allowed for easier treatment of path constraints and curvature.

The proposed controller was tested with a high-fidelity vehicle model on a simulated test track while tracking the track centerline and a space-varying longitudinal velocity reference. Over one lap, the results showed that significant energy savings come from slight reductions in average longitudinal velocity, which are maximized by smoothing longitudinal acceleration. For the specific case when the vehicle deviates from the track centerline, the controller tended to prioritize velocity reference tracking, leading to higher average longitudinal velocity and thus total energy consumption, proving the existence of a trade-off between reference tracking and energy consumption.

Future work includes the proper definition of the target cost and set of the MPC problem to include prior knowledge of the curvature ahead, and thus optimally exploit the full track width. In addition, we plan to implement MPC on vehicle hardware to assess computational aspects.

References

[1] IEA, "Global ev outlook 2023," International Energy Agency, Paris, France, Tech. Rep., 2023.

[2] F. Knobloch, S. V. Hanssen, A. Lam, H. Pollitt, P. Salas, U. Chewpreecha, M. A. Huijbregts, and J.-F. Mercure, "Net emission reductions from electric cars and heat pumps in 59 world regions over time," *Nature sustainability*, vol. 3, no. 6, pp. 437–447, 2020.

[3] A. Biswas and A. Emadi, "Energy management systems for electrified powertrains: State-of-the-art review and future trends," *IEEE Transactions on Vehicular Technology*, vol. 68, no. 7, pp. 6453–6467, 2019.

[4] A. Weißmann, D. Görges, and X. Lin, "Energy-optimal adaptive cruise control combining model predictive control and dynamic programming," *Control Engineering Practice*, vol. 72, pp. 125–137, 2018.

[5] Y. Jia, R. Jibrin, and D. Görges, "Energy-optimal adaptive cruise control for electric vehicles based on linear and nonlinear model predictive control," *IEEE Transactions on Vehicular Technology*, vol. 69, no. 12, pp. 14 173–14 187, 2020.

[6] G. V. Raffo, G. K. Gomes, J. E. Normey-Rico, C. R. Kelber, and L. B. Becker, "A predictive controller for autonomous vehicle path tracking," *IEEE Transactions on Intelligent Transportation Systems*, vol. 10, no. 1, pp. 92–102, 2009.

[7] P. F. Lima, M. Nilsson, M. Trincavelli, J. Mårtensson, and B. Wahlberg, "Spatial model predictive control for smooth and accurate steering of an autonomous truck," *IEEE Transactions on Intelligent Vehicles*, vol. 2, no. 4, pp. 238–250, 2017.

[8] J. Ziegler, P. Bender, T. Dang, and C. Stiller, "Trajectory planning for bertha—a local, continuous method," in *2014 IEEE intelligent vehicles symposium proceedings*. IEEE, 2014, pp. 450–457.

[9] Y. Gao, A. Gray, J. V. Frasch, T. Lin, E. Tseng, J. K. Hedrick, and F. Borrelli, "Spatial predictive control for agile semi-autonomous ground vehicles," in *Proceedings of the 11th international symposium on advanced vehicle control*, no. 2, 2012, pp. 1–6.

[10] J. V. Frasch, A. Gray, M. Zanon, H. J. Ferreau, S. Sager, F. Borrelli, and M. Diehl, "An auto-generated nonlinear mpc algorithm for real-time obstacle avoidance of ground vehicles," in *2013 European Control Conference (ECC)*, 2013, pp. 4136–4141.

[11] Z. Nie and H. Farzaneh, "Energy-efficient lane-change motion planning for personalized autonomous driving," *Applied Energy*, vol. 338, p. 120926, 2023.

[12] F. Micheli, M. Bersani, S. Arrigoni, F. Braghin, and F. Cheli, "Nmpc trajectory planner for urban autonomous driving," *Vehicle system dynamics*, vol. 61, no. 5, pp. 1387–1409, 2023.

[13] X. Chen, H. Mai, Z. Zhang, and F. Gu, "A novel adaptive pseudospectral method for the optimal control problem of automatic car parking," *Asian Journal of Control*, vol. 24, no. 3, pp. 1363–1377, 2022.

[14] X. Liu, A. Fotouhi, and D. J. Auger, "Energy-optimal overtaking manoeuvres of formula-e cars," *Vehicle System Dynamics*, vol. 61, no. 8, pp. 2023–2050, 2023.

[15] L. Claussmann, M. Revilloud, D. Gruyer, and S. Glaser, "A review of motion planning for highway autonomous driving," *IEEE Transactions on Intelligent Transportation Systems*, vol. 21, no. 5, pp. 1826–1848, 2020.

[16] K. Berntorp, B. Olofsson, K. Lundahl, and L. Nielsen, "Models and methodology for optimal trajectory generation in safety-critical road–vehicle manoeuvres," *Vehicle System Dynamics*, vol. 52, no. 10, pp. 1304–1332, 2014.

[17] A. Rucco, G. Notarstefano, and J. Hauser, "An efficient minimum-time trajectory generation strategy for two-track car vehicles," *IEEE Transactions on Control Systems Technology*, vol. 23, no. 4, pp. 1505–1519, 2015.

[18] H. Pacejka, *Tire and vehicle dynamics*. Elsevier, 2005.

[19] R. Verschueren, G. Frison, D. Kouzoupis, J. Frey, N. v. Duijkeren, A. Zanelli, B. Novoselnik, T. Albin, R. Quirynen, and M. Diehl, "acados—a modular open-source framework for fast embedded optimal control," *Mathematical Programming Computation*, vol. 14, no. 1, pp. 147–183, 2022.

[20] G. Frison and M. Diehl, "Hpipm: a high-performance quadratic programming framework for model predictive control," *IFAC-PapersOnLine*, vol. 53, no. 2, pp. 6563–6569, 2020.